



TECHNICAL ARTICLE

# Effect of Ultrasonic Surface Rolling on Fretting Friction and Wear Properties of Heat-Treated Hot Isostatic Pressing Ti-6Al-4V Alloy

Gang Li , Wenkang Zhang, Yu Liu, Xinlei Xiao, Da Song, and Zhuo Xu

Submitted: 9 June 2021 / Revised: 4 November 2021 / Accepted: 15 November 2021 / Published online: 1 December 2021

This work presents the effect of ultrasonic surface rolling process (USRP) on fretting friction and wear properties of Ti-6Al-4V alloy that was prepared by hot isostatic pressing (HIP) before and after heat treatment. The results suggest that the heat-treated HIPed Ti-6Al-4V alloy exhibits higher microhardness and surface roughness values along with a grain size of 200 nm under the same USRP treatment. The thickness of the strengthening surface layer of the heat-treated sample was reduced by 20% compared to the unheat-treated sample on the identical USRP treatments. Meanwhile, it has higher coefficient of friction (CoF) and more severe fretting wear scar. Moreover, the wear debris was contained some large blocks. Additionally, the wear mechanism was mainly abrasive and accompanied by a bonding behavior. The sliding regimes were analyzed by the changes in CoFs and fretting wear scars. In addition, the friction temperature and viscoplasticity were also very important for the fretting friction and wear performance under identical slip conditions. Finally, the heat-treated material after USRP showed a higher wear rate because of the change in microstructure and mechanical properties. This would intensify the friction and wear response between the counter grinding sample and target sample.

**Keywords** fretting friction and wear properties, heat treatment, HIP Ti-6Al-4V alloy, ultrasonic surface rolling

## 1. Introduction

Nowadays, Ti-6Al-4V alloy is the most extensively used titanium alloy material in many industry fields (Ref 1). Although Ti-6Al-4V alloy has outstanding advantages such as high strength and light weight, it still shows the relatively poor properties of friction and wear resistance (Ref 2). This will reduce its service life and performance as a core component and limit its use in other industries. In this regard, the use of a surface modification technology is meaningful and important. It can improve the fretting wear resistance by changing the microstructure (grain size and microdefects) and mechanical properties of the material. In general, the process of heat treatment is also a common method in the industry to improve the mechanical properties by changing the microstructure of metals (Ref 3-5). For instance, Yan et al. studied the effect of heat treatment on the phase transformation and mechanical properties of Ti-6Al-4V alloy (Ref 6). It can be found that

thermo-mechanical treatments allowed to modify the microstructure in the size and shape of the grains, reduce the interior microdefects, as well as change the volume fraction of phases. Zhang et al. also indicated that  $\alpha$  laths became coarser and amount of nano-sized  $\beta$  particles decreased after higher-temperature solution heat treatment (Ref 7). But this method is only limited to improving the overall performance from the material microstructure. However, as a new type of metal surface processing technology, ultrasonic surface rolling process (USRP) becomes more and more deeply researched and applied in material strengthen process (Ref 8). Compared with the conventional cold rolling process, ultrasonic surface rolling can process thin-walled workpieces to improve fatigue life and resistance failure mechanism with slight deformation (Ref 9, 10). Continuous rolling and high-frequency impacting on material surface layer by ultrasonic waves can achieve the purpose of improving the microstructure. The alloy produces a series of substructures at the microlevel such as grain refinement, dislocation walls and deformation crystal twins after USRP treatment. In addition, the mechanical properties of the alloy treated by USRP are also increased and show the good friction and wear resistance (Ref 11, 12). Ren et al. found that the fretting wear resistance of titanium alloy was improved after ultrasonic surface rolling, the microhardness of surface increased about 20%, the compressive residual stress about  $-1000$  MPa occurred, and the wear rate was reduced about 70% (Ref 13). Meng et al. indicated that multistage structure with mm/micro/nano-textures combined with a strengthened layer caused by ultrasonic rolling technology and increased the mechanical and tribological properties of surfaces (Ref 14). Moreover, the synergistic combination of strengthened layer and texture structure could contribute to prolonging the friction and wear life of materials. Therefore, the combination of these

Gang Li, Department of Mechanical Engineering, Northeast Electric Power University, Jilin, China; and Gongqing Institute of Science and Technology, Jiujiang, China; Wenkang Zhang, Xinlei Xiao, Da Song, and Zhuo Xu, Department of Mechanical Engineering, Northeast Electric Power University, Jilin, China; and Yu Liu, Department of Mechanical Engineering, Northeast Electric Power University, Jilin, China; and Nanchang Institute of Technology, Nanchang, China. Contact e-mail: ligang\_scut@outlook.com.

two processes is expected to further improve the overall performance of the material in use based on their own advantages.

This paper is mainly to investigate the fretting friction and wear performance of the heat-treated HIP Ti-6Al-4V processed by USRP treatment. Therefore, the material can produce the high residual compressive stress and microhardness, fine grains deformed layer, reduce the surface roughness, and finally enhance the mechanical properties of material itself. These have a positive effect on improving the tribological performance of the material. Meanwhile, the microstructure and mechanical properties in material surface modification layer are characterized by some microanalytical instruments and techniques. Moreover, the fretting friction and wear properties in dry friction condition are also discussed and specifically analyze the causes.

## 2. Experimental Details

### 2.1 Heat Treatment and USRP Treatment

Ti-6Al-4V alloy bar was fabricated by hot isostatic pressing (HIP) with the pre-alloyed powder. The powder was prepared by electrode induction melting gas atomization (EIGA) technique. The particle size range of this powder changed from 50 to 400  $\mu\text{m}$ . The chemical composition of Ti-6Al-4V alloy is shown in Table 1. HIP processing parameters of Ti-6Al-4V powder were as follows: 850 °C (heating temperature), 50 MPa (vacuum pressure), and 3 h (time). Finally, the density and size of HIP bar were 99.8% and  $\Phi 40 \times 500$  mm, respectively.

The heat treatment of HIP Ti-6Al-4V bar was conducted in the box-type muffle furnace (SX3-3-10) commonly used in the laboratory. The parameters of heat treatment included: The temperature was 900 °C, the holding time was 3 h, and then it was cooled with the furnace.

Ultrasonic surface rolling treatment for HIP Ti-6Al-4V bar was conducted by HK30C ultrasonic surface strengthening equipment. It was mainly composed of cylinder, ultrasonic wave generator, horn, executive agency, transducer, and impact head (the diameter of 10 mm and the hardness of 90 HRA). The bar was fixed on a horizontal lathe and rotated at a certain speed during USRP treatment. Meanwhile, ultrasonic rolling head performed high-frequency shock to strengthen surface layer of the material. The schematic diagram of USRP treatment and the local specific strengthening process is shown in Fig. 1. The parameters of USRP are shown in Table 2.

### 2.2 Surface Characterization and Mechanical Properties

Firstly, Ti-6Al-4V alloy bar was uniformly cut into the specimens with the size of 10 × 10 × 10 mm (kept the strengthened arc surface) in order to conduct a more in-depth study. Then, the samples were prepared using SiC abrasive papers progressively from 180 to 2500 grit, polished the cross

sections, etched in Kroll's reagent, and then washed ultrasonically in acetone for microscopic analysis. SEM (scanning electron microscope) pictures of cross-sectional microstructures were studied by Quanta 200 FEG with a voltage of 20 kV. The size of the grain and phases was measured by Nano measurer. The sample for TEM (Transmission electron microscope) analysis was processed by FIB (Helios nanolab 600 FEI). TEM images and corresponding selected area electron diffraction (SAED) were obtained by using a TECNAI G2 S-TWIN F20 FEI with an accelerating voltage of 200 kV. The microhardness values were measured by MVS-1000Z model hard meter (the load of 0.5 N and the duration of 10 s). Surface roughness and 3D surface profile were measured by BMT SMS expert-level measurement system (scanning speed of 0.1 mm/s and the minimum step size of 0.5  $\mu\text{m}$ ). The Vickers microhardness was measured by MVS 1000D1 at a load of 0.25 N for a dwell time of 15 s. The residual stresses were measured by Rigaku Automate II equipment using the  $\sin^2\psi$  method at a tube current and voltage of 40 mA and 30 kV. The tensile properties were tested by an ultimate tensile testing machine of SANS (E45 and 50 kN) at a speed of 20 mm/min.

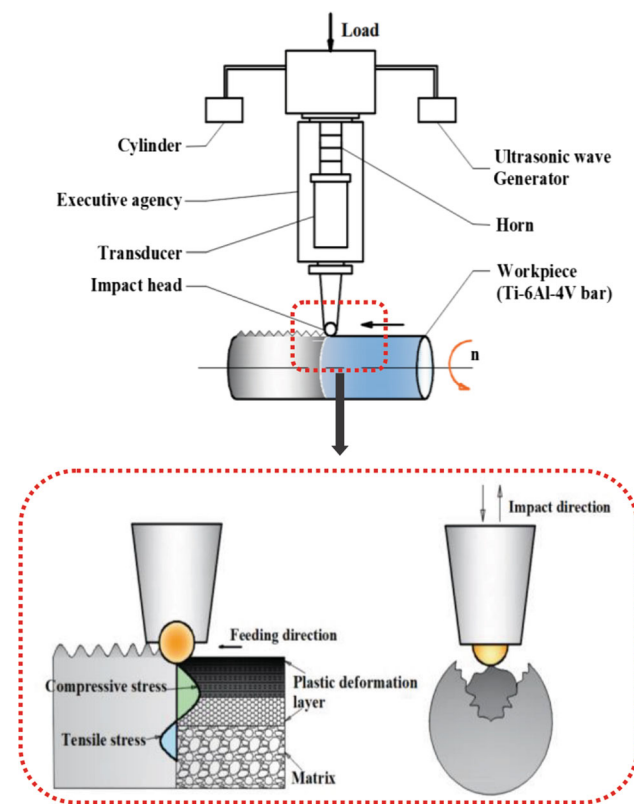


Fig. 1 The schematic diagram of USRP treatment

Table 1 Chemical composition of Ti-6Al-4V alloy (wt.%)

Element	Al	V	Fe	C	O	Si	N	H	Ti
Average	6.0	4.0	0.21	0.08	0.12	≤ 0.05	0.09	0.002	Rest

## 2.3 Fretting Friction and Wear

Fretting friction and wear properties of the samples were researched using a high-frequency oscillating tribometer of SRV-IV (DIN51834) at a temperature of 25 °C against a GCr-15 chrome steel ball with a diameter of 10 mm under dry sliding conditions. The schematic view of fretting tribometer is shown in Fig. 2. The upper ball was loaded radially onto the specimen and oscillated reciprocatingly in the horizontal direction with a slight amplitude (sliding friction without lubrication), while the lower specimen was stationary. In details, the normal load was 10 N, the stroke was 200  $\mu\text{m}$ , the frequency was 10 Hz, the contact pressure was 40 MPa, and the duration time was 30 min. The coefficient of friction (CoF) was automatically recorded during each test by a data acquisition system. GCr-15 chrome steel was selected as a counter grinding material due to its potential to solve the fretting tribological problems in various aerospace mechanical and biomedical components (Ref 15). Each test was conducted three times to minimize the data scattering. Meanwhile, each specimen was ultrasonically washed in acetone for 10 min before and after the test. To contrast wear resistance of Ti-6Al-4V alloy before and after heat treatment, wear debris was collected, and EDS and SEM were used to analyze the change of composition and shape.

## 3. Results and Discussion

### 3.1 Microstructure

The micrographs from the cross section of the specimen, processed for different conditions are provided in Fig. 3. The distribution of phase in the microstructure of the untreated sample (Fig. 3) is relatively uniform, and there is no obvious distribution trend between phases. The interior of the material is mainly composed of lamellar  $\alpha$  phase, intercrystalline  $\beta$  phase, and several tiny pores (the white arrows). Material surface layer has an obvious plastic distribution after USRP treatment such

as the phenomenon that the grain shows a 45° inclined distribution form (Fig. 3b) and the angle tends to be consistent with the feed direction. However, the microstructure away from surface modification layer is like Fig. 3(a) and presents a messy distribution, and there is no significant plastic deformation. This is because that the effect of ultrasonic surface rolling is restricted to the strengthening of material surface layer (the depth of tens of microns) and cannot produce the obvious dislocation and plastic deformation impact on the grains deeper in the material. Therefore, the degree of material plastic deformation in surface modification layer gradually decreases as material depth increases. It is obvious in Fig. 3(b) that  $\beta$  phase (BCC) has become relatively curved and is squeezed into  $\alpha$  phase (HCP) within a few micrometers from material surface because of its own lattice structure (BCC). Generally, the BCC lattice structure has more slip systems and is prone to produce the larger plastic deformation than the HCP lattice structure. Now, the aspect ratio of  $\alpha$  and  $\beta$  phases in surface modification layer is 4.95 and 8.43, respectively. Meanwhile, the density of material surface modification layer is obviously increased owing to the effects of ultrasonic vibration and rolling. In addition, the micropores and cracks in material surface modification layer can effectively be closed by USRP treatment and reduce the microscopic defects compared with the internal material matrix. The significant thickness of material plastic deformation layer in Fig. 3(b) is about 40  $\mu\text{m}$ . However, the phases in Fig. 3(c) are obviously grown up and form more equiaxed phases after heat treatment. A part of  $\beta$  phase is transformed into  $\alpha$  phase, and the secondary  $\alpha$  phase is produced. Of course, the high heat treatment temperature will also make  $\alpha$  phase grow up. The aspect ratio of  $\alpha$  and  $\beta$  phases in surface modification layer is decreased to 2.59 and 6.65, respectively. The shape of  $\alpha$  phase gradually changes from lamellar to globular after heat treatment. Finally, the area ratio of  $\alpha$  phase is increased (approximately 8%) and results in improving material mechanical properties (Ref 16). Meanwhile, the appropriate heat treatment process can effectively improve the uniformity and internal stress inside the material. The changes of microstructure and properties of heat-treated

**Table 2** Parameters of ultrasonic surface rolling process

Rolling pressure, N	Frequency, Hz	Amplitude, $\mu\text{m}$	Spindle speed, rpm	Feed rate, mm/rev	Head diameter, mm
900	30	10	200	0.05	10

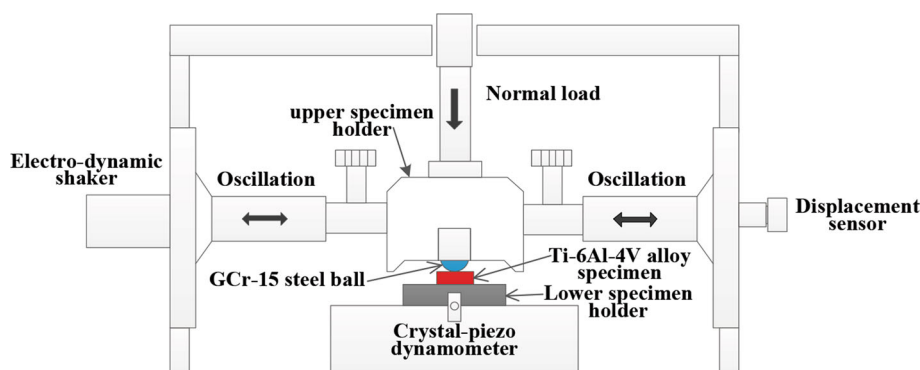


**Fig. 2** The schematic diagram of fretting friction and wear test

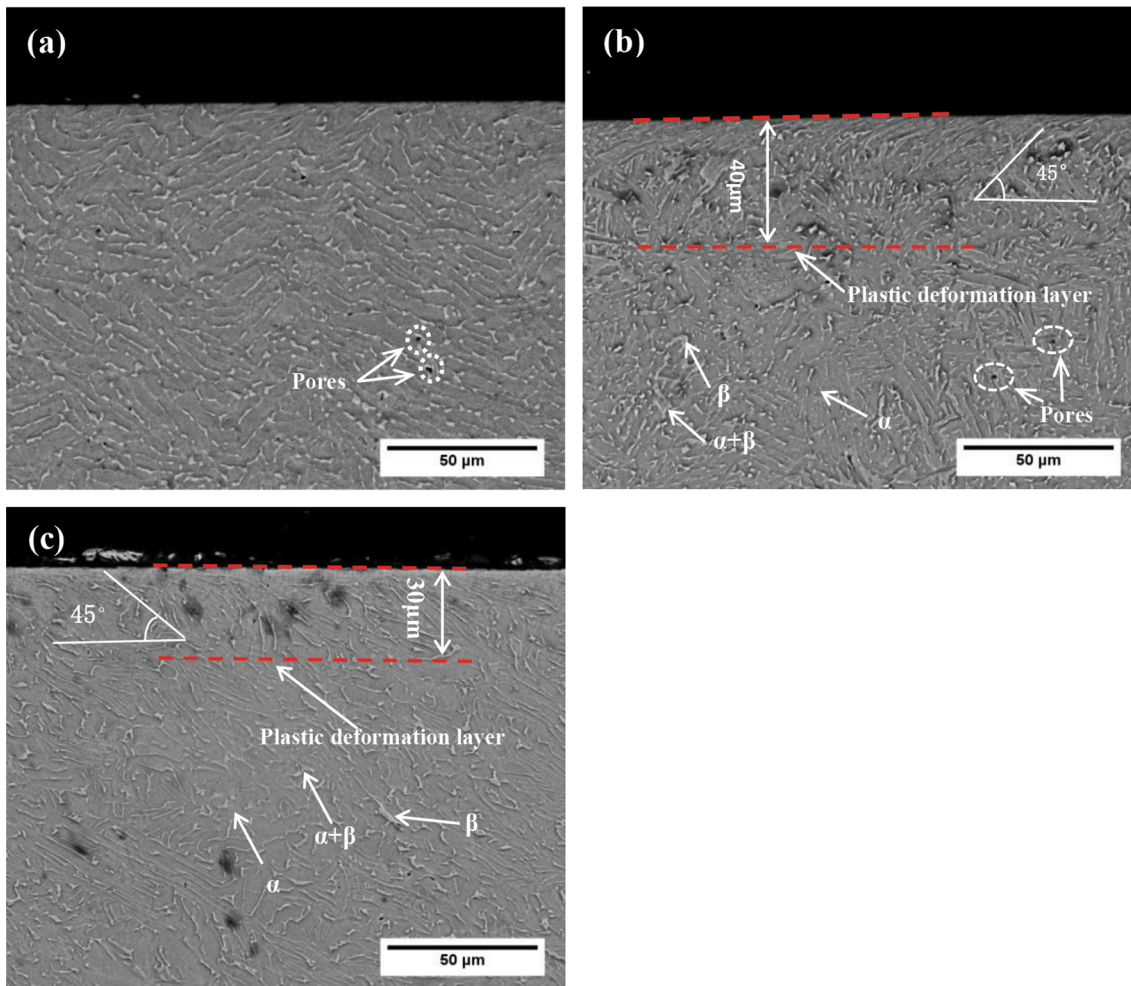


**Fig. 3** Cross-sectional SEM images of the samples treated by different processing conditions: (a) the untreated sample; (b) the unheat-treated sample treated by USRP; (c) the heat-treated sample treated by USRP

material will affect the strengthening effect of USRP treatment in material inner (Ref 17). It can be found that the thickness of surface strengthening layer of the heat-treated sample after USRP treatment becomes comparatively thin and only has about 30  $\mu\text{m}$  (Fig. 3c) due to the HCP structure of  $\alpha$  phase. This will bring some certain obstacles to the effect of ultrasonic surface rolling strengthening. Moreover, the good influence of ultrasonic surface rolling on the internal microdefects of the material will also be weakened.

The TEM analysis of surface modification layer in Fig. 3(b) and (c) is shown in Fig. 4. The grains in the top layer of Fig. 4(a) are significantly refined, and the size changes from the initial hundreds of micrometers into the current sub-micrometer (about 200 nm) (Ref 18). It can be found that most of the grains are equiaxed with the random orientation and no regular arrangement. Generally, the slip capacity of the grain boundary is related to the dislocation movement and increases with the increase of the orientation difference. The grain interior is composed of the dense dislocation entanglements (the black arrows). The grain boundary is not very clear, and the plastic deformation is mainly achieved by the movement of dislocations. Now, material top layer has occurred a large plastic deformation. Meanwhile, the fine grains are formed at the

intersection of sub-grain boundaries as strain and strain rate increase (Ref 8). In the process of sub-grains forming, the migration and rearrangement of dislocations in the different regions of the grains gradually cause the regions to be “divided” and form the “cell blocks.” The specific process is as follows: First the dislocation configuration tends to combine spontaneously to a lower-energy state because of deformation twinning, then the boundary of cell block becomes sharp due to twin intersections and twin-dislocation interactions, and finally subgrain boundaries are gradually formed. The electron diffraction pattern of area “1” in Fig. 4(a) manifests some small segments of the continuity diffraction rings. This indicates that there are the grains and sub-grains co-existing in this area. As the depth from material surface increases further, the grain with low dislocation density gradually becomes a slip band-like structure with high dislocation density (the black arrows in Fig. 4b) at the depth of 6  $\mu\text{m}$ . Here, the plastic deformation of the material is reduced, and the dislocations become more concentrated. The electron diffraction pattern of area “2” in Fig. 4(b) shows a regular lattice structure. At this moment, the plastic deformation of the material mainly occurs at the boundary or interior of the grain and there is no obvious effect of grain refinement. TEM

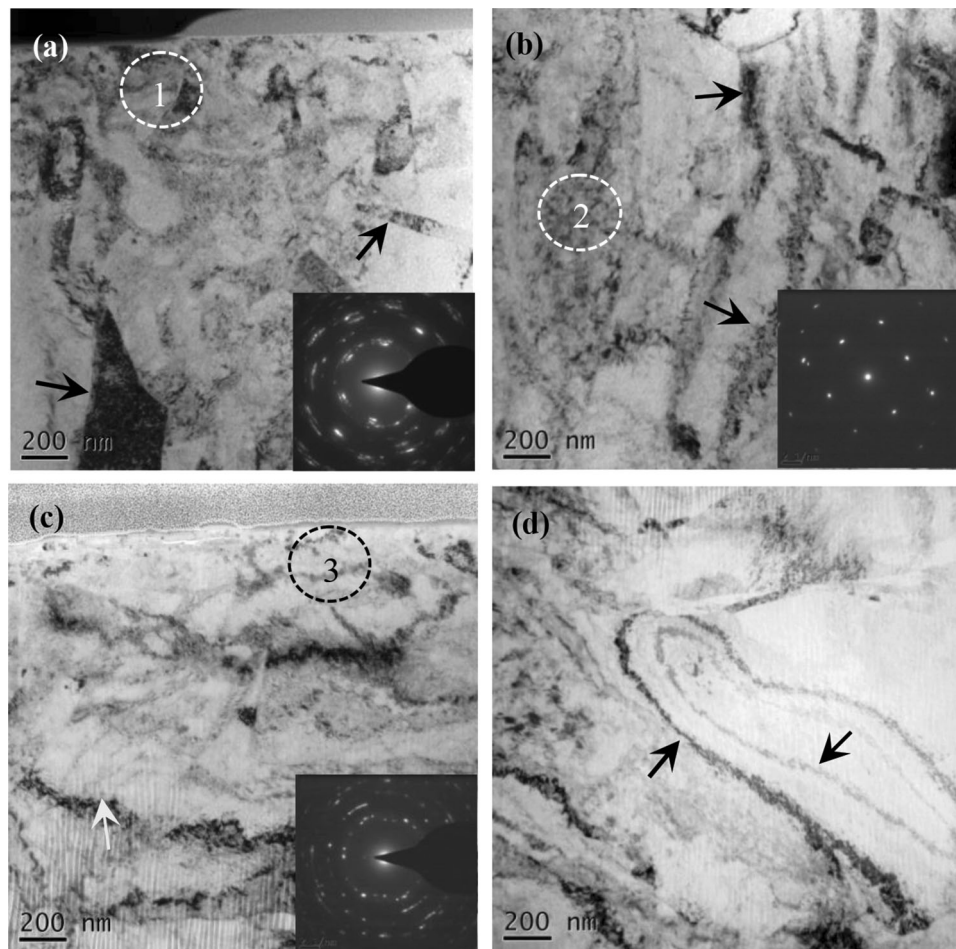
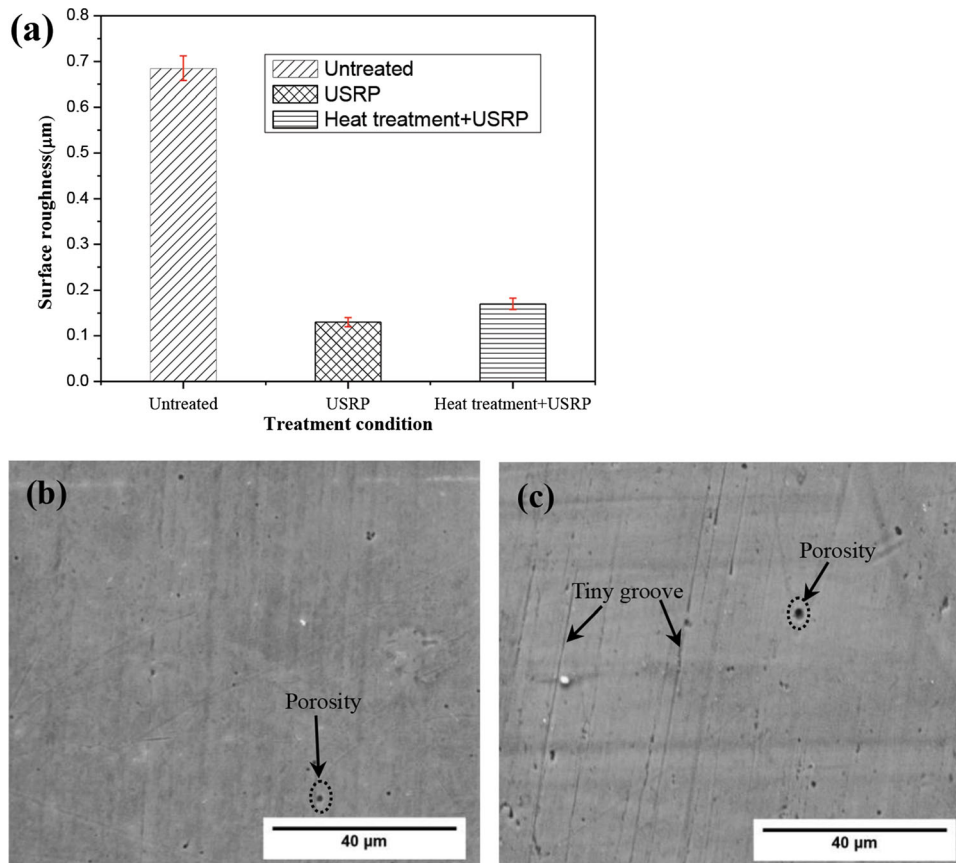


**Fig. 4** TEM figures at different depths of the samples: (a) the depth at 2  $\mu\text{m}$  of the unheat-treated sample treated by USRP; (b) the depth at 6  $\mu\text{m}$  of the unheat-treated sample treated by USRP; (c) the depth at 2  $\mu\text{m}$  of the heat-treated sample treated by USRP; (d) the depth at 6  $\mu\text{m}$  of the heat-treated sample treated by USRP

pictures of surface modification layer for the heat-treated sample treated by ultrasonic surface rolling are shown in Fig. 4(c) and (d). The effect of grain refinement in surface modification layer has a little worse in Fig. 4(c) because of the change of phases caused by heat treatment. The size of the grains is mostly a few hundred nanometers (about 400 nm) and obviously larger than that shown in Fig. 4(a), and the grain boundaries are also blurry. But some strips of deformed grains can still be seen as indicated by the white arrow in Fig. 4(a). Moreover, the dislocation density is declined compared to Fig. 4(a), and there is no large area of dislocation entanglement. The electron diffraction pattern of area '3' in Fig. 4(c) shows that the analysis result is a discontinuous spot and there is a small continuity occasionally. Therefore, the selected area still contains multiple grains. These also illustrates that the heat-treated material has the smaller plastic deformation degree and poorer grain refinement in the same USRP treatment conditions. However, the dislocation density (indicated by the white arrows) in Fig. 4(d) is further reduced and the dislocation width also significantly decreases compared to Fig. 4(b). The black ring-shaped area (indicated by the black arrow) may be the fringe phenomenon of the dislocation. Now, the plastic deformation of material is relatively slight and uniform and mainly occurs at grain boundaries. They should be the so-called extensional contours of grain deformation. Now, the dislocations have no effect of grain refinement (Ref 19, 20).

### 3.2 Surface Roughness and Mechanical Properties

The change of surface roughness provided by the samples under different processing conditions is shown in Fig. 5(a). It can be found that surface roughness exhibits a large change range before and after USRP treatment. The smallest value of surface roughness is 0.13  $\mu\text{m}$  that is obtained by the sample treated by USRP. The surface of USRP-treated sample in Fig. 5(b) is relatively smooth with no obvious defects, and there are only a few tiny porosities. However, surface roughness of the untreated sample is apparently higher than this value. This is mainly due to the grooves produced by the process of cutting on material surface. But, the grooves become very flatness in Fig. 5(b) by the combined action of the high-frequency ultrasonic impacting and continuous rolling. This also indicates that the sample undergoes the large and symmetrical plastic deformation in unit area so that it can reduce surface roughness more effectively. However, the value of surface roughness of the heat-treated sample treated by USRP treatment is increased to 0.17  $\mu\text{m}$  on account of the change of the constituent phases. Moreover, it will improve the microhardness and yield limit of the material and bring some resistance for the material's elasto-plasticity. In general, the good surface quality will further increase the properties of the sample and can avoid or delay the occurrence of the initial crack and stress concentration. The surface of the heat-treated sample after USRP treatment in



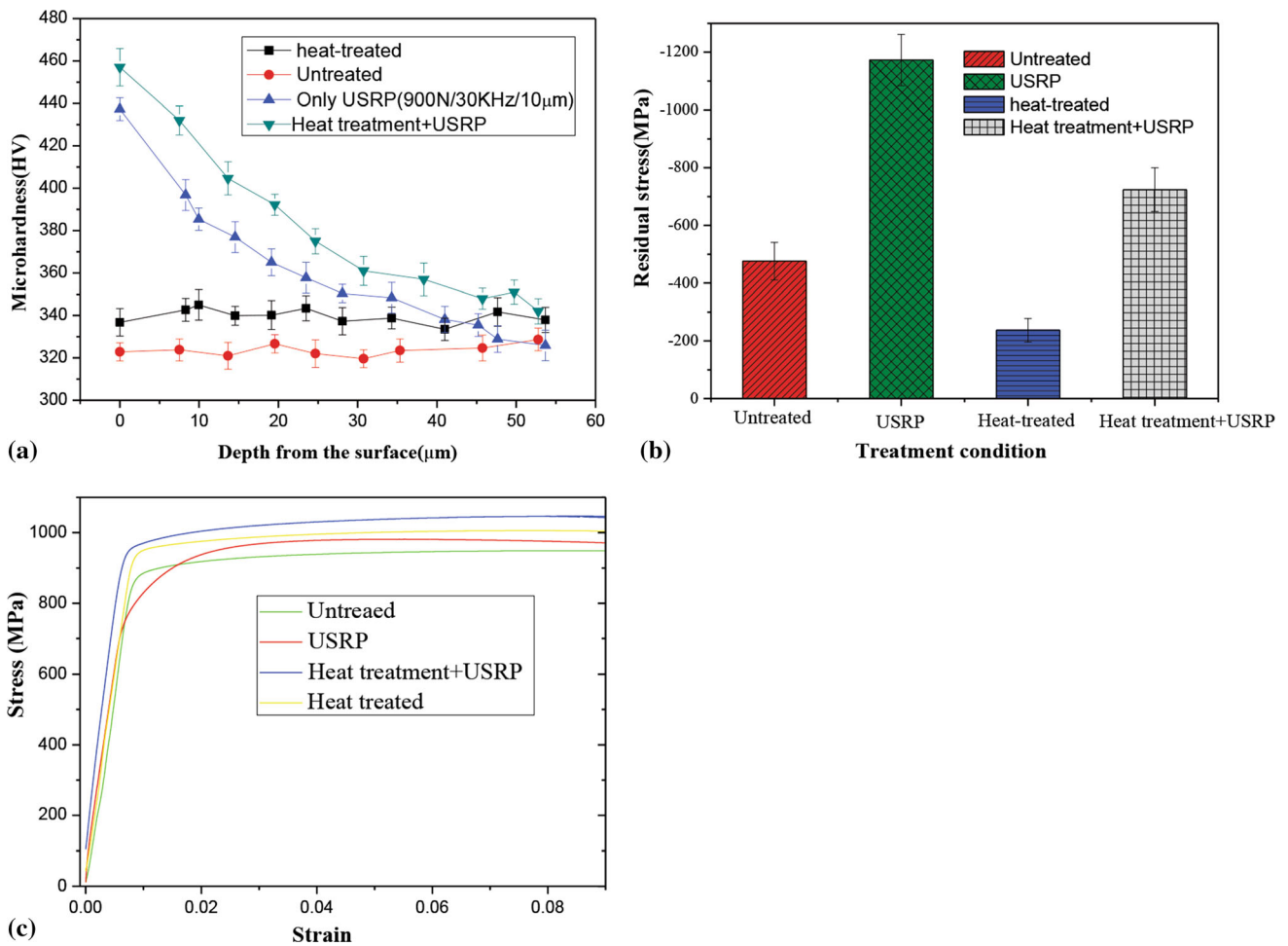
**Fig. 5** The change of surface roughness and morphology: (a) surface roughness of the samples under different treatment conditions; (b) surface morphology of the unheat-treated sample treated by USRP; (c) surface morphology of the heat-treated sample treated by USRP

Fig. 5(c) has some tiny groove scars and porosities. Although the grooves can be filled by material plastic flow produced by ultrasonic surface treatment, it cannot smooth completely the grooves and close the micropores on material surface. Finally, these factors result in a reduction of the plastic deformation of the material and decline the surface roughness of the sample.

The measured results of microhardness are exhibited in Fig. 6(a). The microhardness values gradually decrease as the depth of the material increases until it is consistent with the microhardness of material matrix. The microhardness values of the heat-treated sample are increased to 342 HV from the initial 323 HV. Furthermore, there is an about 20 HV difference in the microhardness of the material before and after heat treatment under the same USRP treatment conditions. The process of heat treatment promotes the transformation of some  $\beta$ -phases into  $\alpha$ -phase and primary  $\alpha$ -phase and produces some columnar grains, which leads to an increase in the microhardness of the material. Surface strengthening layer produced by USRP treatment can further resist the plastic deformation of the material during microhardness measurement. So, surface microhardness values of the heat-treated sample are increased from 438 to 457 HV compared to the unheat-treated sample under the same USRP treatment. Generally, the initial microhardness of the material has a direct effect on ultrasonic surface rolling strengthening. The higher initial microhardness of the material makes surface-modified layer also show a higher microhardness value after USRP treatment. Moreover, the high microhardness of the material will increase the deformation resistance of the

material during USRP treatment and result in a smaller hardening depth for the heat-treated sample after USRP treatment. Of course, the microhardness of the material is also related to the grain size and residual stresses, etc. But it is mainly affected by the composition structure of material itself.

Figure 6(b) shows the residual stresses of the samples treated with different conditions. As can be observed from the histogram, the unheat-treated sample has the larger compressive residual stress than the heat-treated sample under the same USRP treatment. In general, the residual stress is directly related to the plastic deformation of the material. The compressive residual stress existed in the surface of untreated sample mainly comes from the cutting deformation of the material. Meanwhile, the process of heat treatment reduces the residual stress inside the material which comes from the cutting. Moreover, the increase of  $\alpha$  phase after heat treatment declines the ability of material plastic deformation. Finally, the heat-treated sample after USRP treatment shows a relatively low residual stress value. This also indicates that the heat-treated material after USRP treatment has the smaller plastic deformation. The high compressive residual stress can help improve the resistance of material surface to fretting wear. In addition, it also shows that USRP treatment has a good effect of surface strengthening (Ref 21). The plastic deformation in surface modification layer should be attributed to many dislocations' generation and movement. Therefore, it can be inferred that the depth of compressive residual stress is corresponding to the depth of dislocation generation region (Ref 22).



**Fig. 6** The microhardness and residual stress: (a) the microhardness along the direction of depth; (b) the residual stress at material top layer; (c) the stress–strain curve of the tensile samples

**Table 3** The tensile properties of the samples treated by different conditions

Treatment conditions	Tensile strength, MPa	Yield strength, MPa	Rate of reduction in area, %	Elongation, %
The untreated sample	963	903	41.7	22
The sample treated by USRP	990	924	51.7	19
The heat-treated sample	1005	921	43.8	16.5
The heat-treated sample after USRP	1045	949	12.9	3.4

The tensile properties of the samples are shown in Fig. 6(c) and Table 3. Obviously, compared with untreated samples, the tensile strength and yield strength of heat-treated samples after USRP treatment are increased to 1045 and 949 MPa. There is an increase rate of 8.5 and 5.1%, respectively. The stress–strain curve has the highest location in Fig. 6(c) and shows the less plastic deformation during tensile test. But, the increase rate is decreased to 5.6 and 2.7% for the sample treated by USRP. It demonstrates a more uniform deformation process at the inflection point of the curve in Fig. 6(c). This indirect indicates that it is feasible to further improve material's properties through the combining heat treatment and ultrasonic surface rolling process. The process of heat treatment can change the structure and proportion of the phases. So, the tensile strength and yield strength of heat-treated samples are increased to 1005

and 990 MPa from the initial 963 and 903 MPa. These values are slightly higher than the tensile properties of the sample treated by USRP, which also indicates that the heat treatment process can be effective in improving the tensile properties of the material. A fine-grained strengthening layer is formed in the surface of the material by USRP treatment. Meanwhile, USRP treatment can improve the state of strain, stress, and energy in material surface layer and delay the occurrence and expansion of microcracks of the sample during tensile test (Ref 23). These explain why the heat-treated sample after USRP treatment has the good tensile properties. However, the rates of sectional shrinkage and elongation of the heat-treated sample after subjected to USRP treatment are reduced to 12.9 and 3.4% with respect to the other samples. This also demonstrates that the changes in the microstructure of the material have a direct

effect on the plastic deformation of the sample during tensile test. On the one hand, the increased  $\alpha$  phase by heat treatment reduces the plastic deformation of the material. On the other hand, surface modification layer produced by USRP treatment will also delay the generation of crack initial point and reduce the proportion of material plastic deformation in initial fracture zone. As a result, when the sample reaches its yield limit in the tensile test, it has a small plastic deformation and produces an instantaneous fracture.

### 3.3 Fretting Friction Coefficient

In generally, the sliding friction regime of the sample can be divided into the partial slip regime, gross slip regime, and mixed slip regime (Ref 24). The coefficient of friction (CoF) is an indirect manifestation of material friction regime. It can be divided into three stages in Fig. 7(a) according to the change trend. “I” is the initial contact stage, and the load is gradually applied to counterbody. The CoFs show a brief upward and downward trend before the sample is in full contact with the counterface. The initial contact under the gross slip condition will modify its elastic response to reach the less dissipating partial slip situation. Such an evolution will be controlled by an increase of the CoF. The initial surface roughness plays an important role in controlling the running-in and steady-state periods, and it ascertains the true contact mode and contact area between two mating surfaces. The high CoF of untreated sample can be attributed to the rough surface which is mainly composed by the grooves from cutting. This will intensify the effect of plowing and increase the fluctuation of CoF. “II” indicates that the contact area between the sample and counterbody is gradually increased and the contact mode changes from point to face. Now, the localized fracture generated in material surface layer before running-in stable period and the wear particles remaining within the contact area may be responsible for the relatively high fluctuation of CoFs. The fretting mixed slip regime is controlled by a further increase of CoF and changes from a low gross slip friction coefficient value up to a stabilized high CoF under partial slip. It also implies a more elastic response of the material. A steady state is obtained with a lowest dissipated energy when the local friction coefficient reaches a maximum value. “III” shows that the friction behavior of the samples has entered the stable stage

and the CoFs maintain a relatively stable state. The declined friction coefficient of the specimens may be attributed to the formation of a tribolayer at the interface due to the joint action of wear debris, oxidation behavior along with mild wear, and the elemental transfer of mating surfaces. The CoFs are significantly lower than the transition value due to the presence of a third body. Such a stable evolution could be explained by the third body smoothing effect. However, a rough surface makes it easier for the wear debris generated during the sliding to escape from the contact interface, thus minimizing the third-body effect. The lowest fretting CoF of the sample treated by USRP treatment should be attributed to the increased mechanical properties, the refined grains, and the declined surface roughness in material surface strengthening layer. These factors will improve the friction response of the sample. But the steady-state CoF of the heat-treated sample treated by USRP treatment is close to that of the untreated sample (Fig. 7b). This is because the mechanical properties of the sample increased significantly after heat treatment coupled with USRP treatment. Although surface modification layer is thinner, the high mechanical properties in material surface layer will intensify the friction behavior and raise the curve of CoF (Ref 25). The samples treated by USRP treatment take the less time to get into the steady state of CoF than untreated sample and keep the lower location. This illustrates that surface strengthening layer produced by USRP treatment can reduce the plowing effect of counterbody and accelerate its friction behavior. Meanwhile, the accumulation of wear debris between the friction faces can also affect the location and fluctuation of CoFs. In addition, the residual stress and strain energy are also the important factors in improving the friction performance.

### 3.4 Fretting Wear Scars and Wear Debris

The wear scars of the samples after fretting friction and wear test are shown in Fig. 8. Generally, the fretting damage can be produced by material adhesion, abrasion, and fatigue. The wear scar in Fig. 8(a) is comparatively flat and mainly composed by the sliding areas, tiny grooves, pits, and delamination. The main wear mechanism is sliding wear and accompanied by abrasive wear and material peeling. Heredia et al. indicated that there was no wear in partial slip regime, and it only appeared at the end of the mixed fretting regime and later during the gross slip

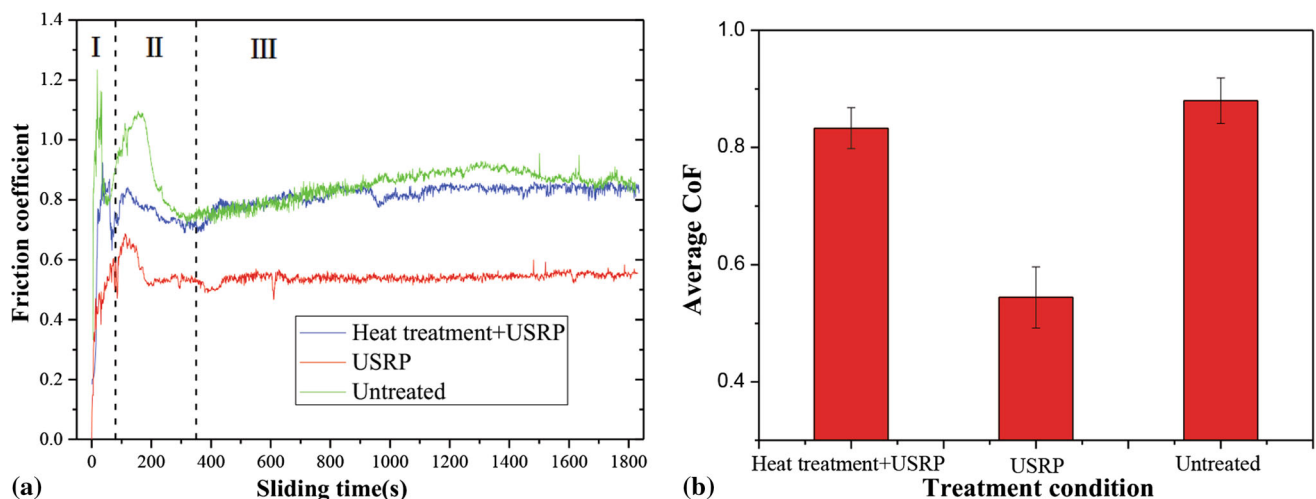
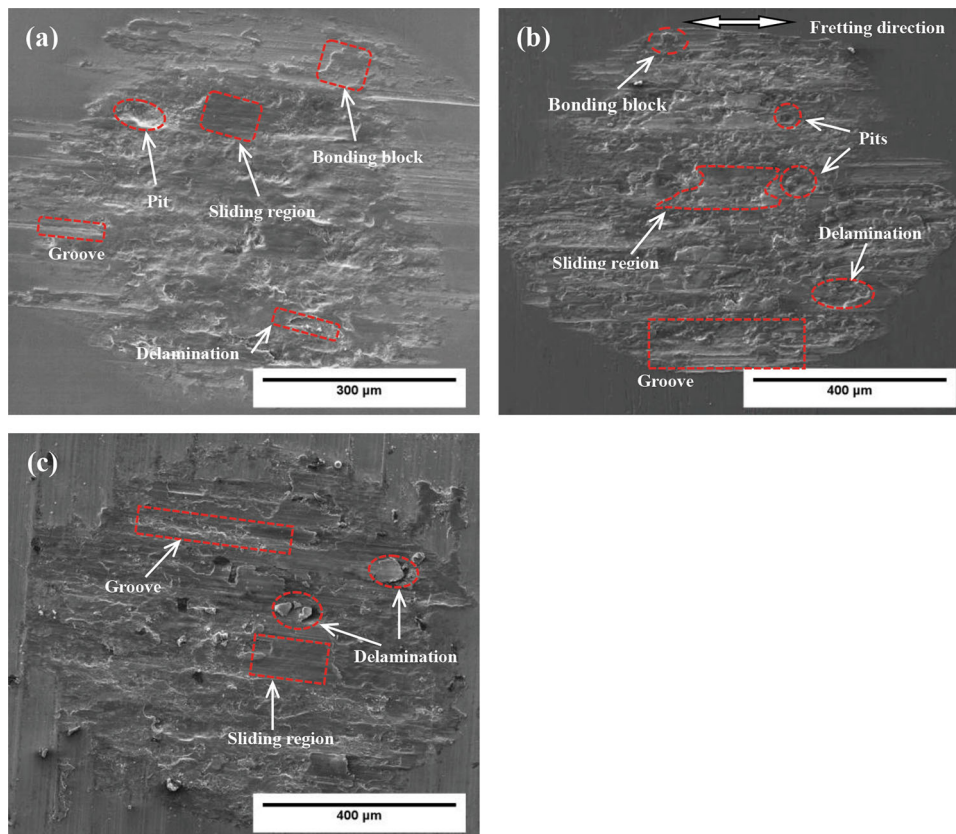


Fig. 7 The CoFs of the samples treated by different conditions: (a) the change of CoFs with the increase of test time; (b) the average CoFs





**Fig. 8** The fretting wear scars of the samples treated by different conditions: (a) the untreated sample; (b) the unheat-treated sample treated by USRP; (c) the heat-treated sample treated by USRP

regime (Ref 24). The partial slip conditions develop the highest stress levels that can induce fatigue crack nucleation and develop the cracking. Meanwhile, the plasticity in partial slip conditions has a significant and complex effect on the evolution of sticking and slip zone sizes and on surface tractions. However, the tangential motion under gross slip conditions promotes plastic shearing across a wide region, leading to the accumulation of plastic strain and delamination cracking. But the transition from partial to gross slip condition can be defined by an energy discontinuity analysis and partly controlled by the adhesion and metal transfer phenomena. There is a gray area around the wear scar and existing some bonding blocks in Fig. 8(a). The behavior of material bonding mainly comes from the high temperature produced by the high speed and cycle dry friction. Moreover, the good plasticity of material matrix can also decline the abrasive and spalling wear, but it is prone to produce adhesion behavior. The high plastic strain mainly results from the sliding condition, and the high contact pressure can be introduced by plowing effect. Then, the process of abrasive wear is activated. The wear sharply reduces both pressure and shear stress by extending the contact area, which are the driving factors of the crack nucleation and crack propagation processes. These will be helpful to produce the grooves and delamination wear. In addition, the tribolayer at the interface will be formed by the increase of local temperature in fretting contact area due to the frictional power dissipation. The tribolayer is also tending to be the more adhesive and plastic sustaining the sliding friction with not obviously spalling. Besides, the lower surface roughness and higher microhardness and compressive residual stress can reduce the wear of the

target sample. The grooves and pits are significantly increased, and the sliding region is decreased for wear scar (Fig. 8b) of the heat-treated sample treated by USRP treatment. Now, the abrasive wear plays a major role and aggravates the wear of the target sample. The higher surface roughness and microhardness and lower compressive residual stress produced by the combination of heat treatment and USRP will intensify the wear behavior of the counter grinding sample to the target sample. This also explains why the CoF shows the relatively high location. At this moment, material bonding behavior becomes very slight and the grooves in Fig. 8(b) are already obvious. Some grooves point toward sub-mechanisms of “Abrasion,” but most of the worn areas show “Delamination” as well as maybe remains of “Mechanical Mixing.” The groove in the wear scar of Fig. 8(c) has become narrow and small, and some broken pieces of material are about to flake off the wear surface. Some slipping areas also exist in Fig. 8(c), but there are no visible large pits. This also illustrates that the wear mechanism of untreated sample is the sliding wear and material spalling, and the proportion of abrasive wear is relatively small. As the test time increases, material surface layer undergoes cyclic plastic deformation, and some fatigue spalling will be produced under the action of reciprocating shear stress. Therefore, it can conclude that surface roughness, yield limit, and residual stress have an important effect on material’s wear behavior. In addition, the grain size can also greatly improve the wear resistance of the sample.

The wear scars of counter grinding samples are shown in Fig. 9. The frictional work should be characteristic for the driven mechanisms that require plastic deformation as will be

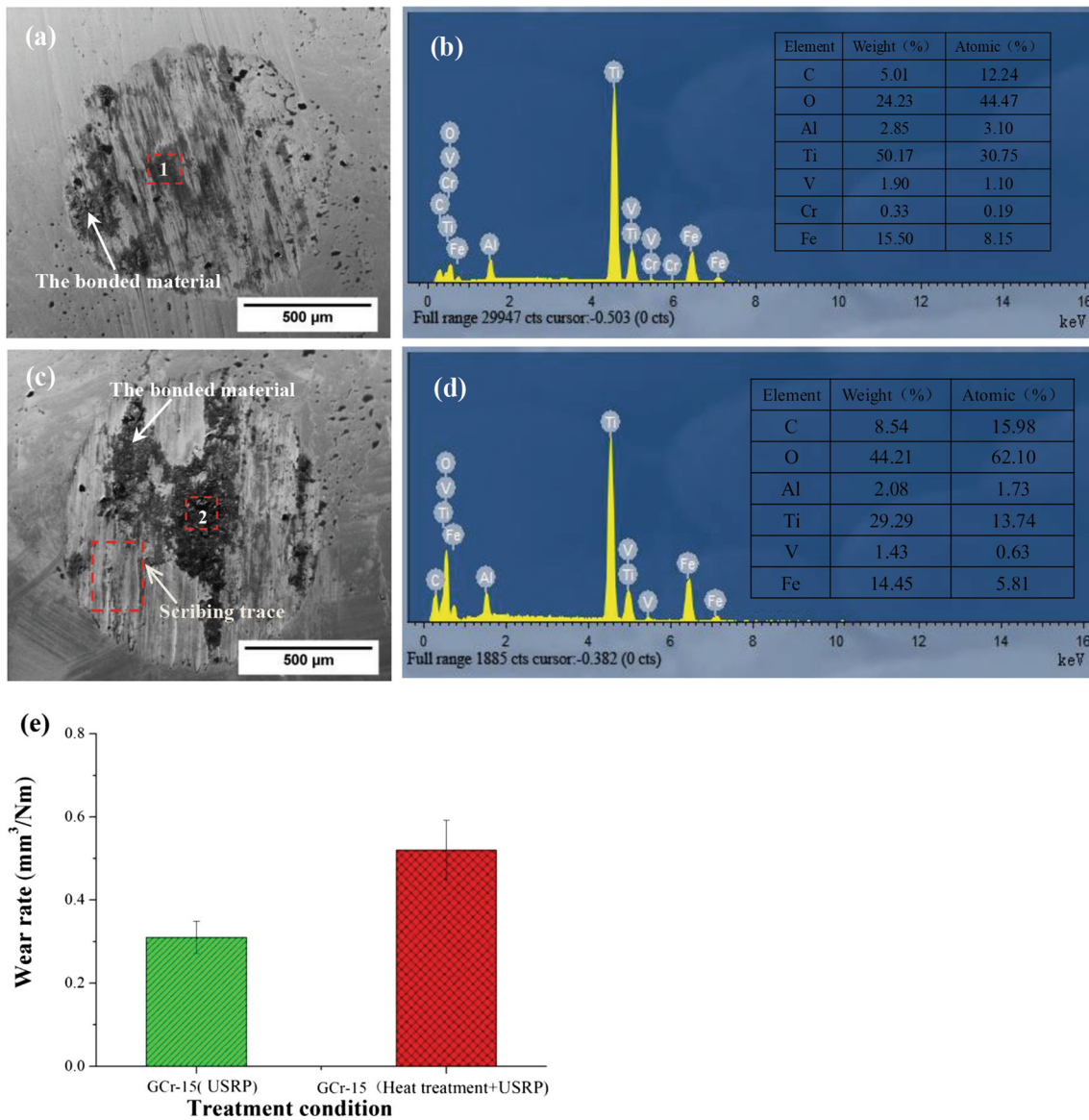


**Fig. 9** The fretting wear scars of GCr15 ball: (a) GCr15 ground with the unheat-treated sample treated by USRP; (b) EDS analysis of area “1”; (c) GCr15 ground with the heat-treated sample treated by USRP; (d) EDS analysis of area “2”; (e) the wear rate of GCr15 ball

mainly the “Microplowing.” So, the wear surfaces in Fig. 9(a) and (c) show some grooves instead of indentations. Generally, the grooves are the characteristic for “Abrasive wear,” which counteracts “Mechanical Mixing” by removing the tribomaterial at every stroke. The shallow grooves without any sharp bounds point toward “Microplowing,” which mostly result in plastic deformation and only a small amount turn into wear particles. When the material undergoes some severe plastic deformation (fractured floes), it will prompt the obvious “Material Transfer” causing “Adhesion.” But there are no obvious signs of delaminations in Fig. 9(a) and (c). The wear scar in Fig. 9(a) is provided by GCr15 ball, and it is tested with the sample treated by USRP treatment. The wear surface is comparatively smooth and there is only less and uniform bonding material. The tiny grooves can be found in Fig. 9(a). This also indirectly indicates that the wear debris is relatively fine and uniform, and the target sample is not suffered the

severe wear. Therefore, the main wear mode is sliding wear. The EDS analysis of area “1” in Fig. 9(b) reveals the elemental composition of material bonding block. The result shows that the composition in area “1” mainly includes Ti, O, and Fe. However, some of the oxygen content comes from the air, as the high friction temperature causes titanium alloy to absorb oxygen elements from the air. The C and Cr elements mainly come from the counter grinding sample. When the heat-treated sample treated by USRP treatment is tested with GCr15 ball, the wear scar in Fig. 9(c) shows some large bonding blocks and scribing trace. This shows that the particle of wear debris should be coarse. In general, the material bonding behavior is related to the wear resistance and viscoplasticity of the material and the friction temperature. When the size of the bonded material reaches a certain degree, it will peel off from the worn surface and form a large piece of wear debris. The EDS analysis of area “2” in Fig. 9(d) contains the more O element. It

demonstrates that the friction temperature between the target sample and the counter grinding sample is comparatively high, and the wear debris can absorb the more oxygen from the air. The interfacial tribolayer mainly consists of wear debris and oxide wear particles. Moreover, the tribomaterial inside the grooves may not be easy to escape during the test and will be welded to the surface of the counterbody in the high-temperature environment. The Cr element is absence in Fig. 9(d). It can be judged that the target sample has occurred severe wear. Meanwhile, GCr15 ball tested with the heat-treated sample treated by USRP also has the higher wear rate in Fig. 9(e). This should be attributed to that the improved microstructure and mechanical properties of heat-treated sample enhance the scratching and plowing effects of the abrasive particles and decline the self-lubricating behavior of the material.

Wear by the debris formation was shown to be the most critical damage phenomenon under gross slip conditions. When the gross sliding plastic deformation has sufficiently accumulated, the delamination wear will be appearance. Then, the delaminated material becomes the debris that will promote the wear in the contact region. The wear debris in Fig. 10(a) is obtained by grinding the USRP-treated sample with GCr15 ball. It is mainly the relatively fine particles, but also contains some small pieces which come from material spalling. The shape and amount of fretting wear debris are primarily determined by the wear mechanism, displacement amplitude, and load. The fine wear debris usually comes from the sliding wear. Of course, the wear resistance and viscoplasticity of the target sample are also very important under the same slip conditions. The wear debris in Fig. 10(c) is produced by grinding the heat-treated sample treated by USRP with GCr15 ball. Some large block-shaped wear debris can be found, and they are produced by the abrasive wear and material bonding

and delamination. The process of heat treatment declines the plasticity of material, which has a great influence on the formation process of wear debris. In addition, the high-temperature environment generated by the high-speed and cycle dry friction will also promote a part of wear debris to stick together into blocks and are welded on the worn surface (Fig. 11). The EDS analysis of area “1” in Fig. 10(b) contains the more Ti and O element and the less Cr element. It reveals that most of wear debris is principally formed by the target sample. But the EDS analysis manifests that the composition of area “2” in Fig. 10(d) increases the C, Cr, and Fe content. They mainly come from GCr15 ball. So, it can be concluded that the counter grinding sample has occurred severe wear behavior. Furthermore, this will also aggravate the wear of the target sample. The part of O element content is rooted in the oxidation of Ti-6Al-4V material during fretting friction and wear test.

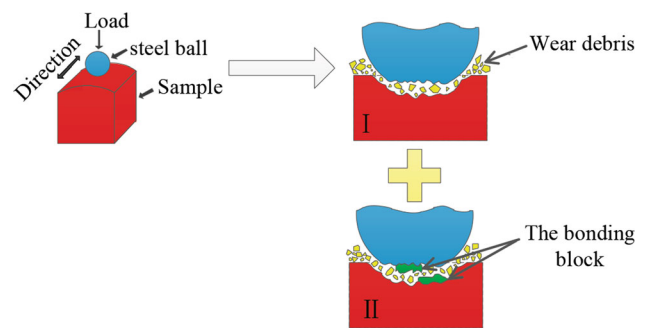


**Fig. 11** The schematic diagram of ejection and bonding behavior of wear debris

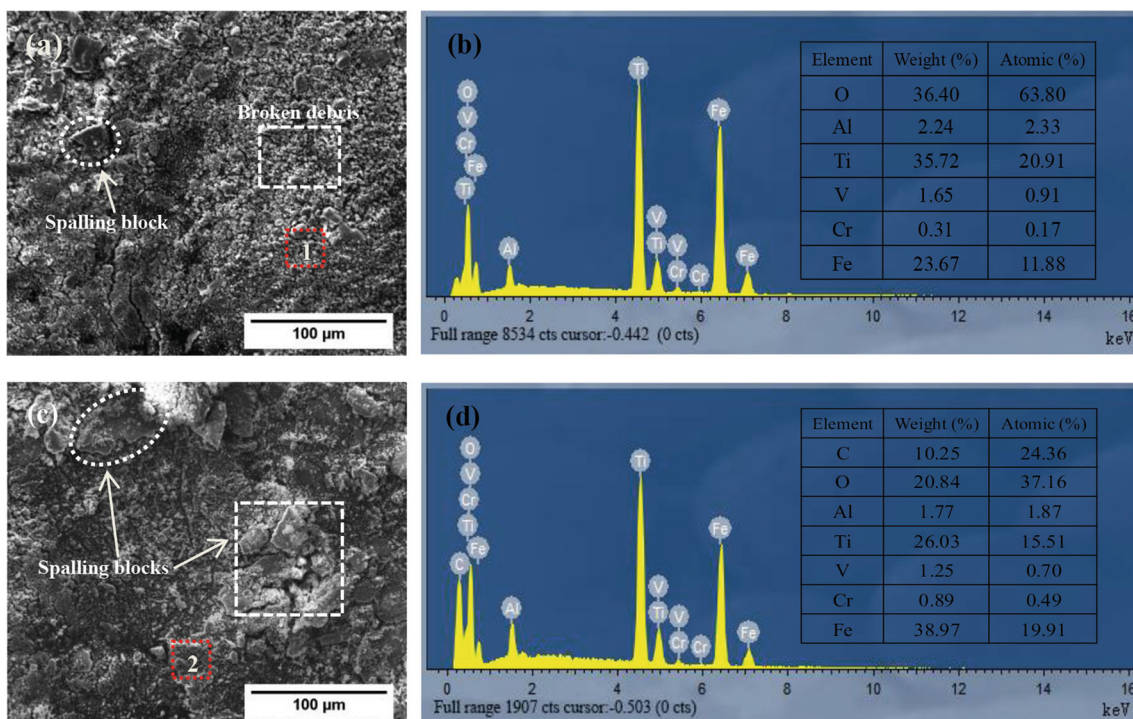


**Fig. 10** SEM image and EDS analysis of wear debris: (a) wear debris provided by the unheat-treated sample treated by USRP; (b) EDS analysis of area “1”; (c) wear debris provided by the heat-treated sample treated by USRP; (d) EDS analysis of area “2”

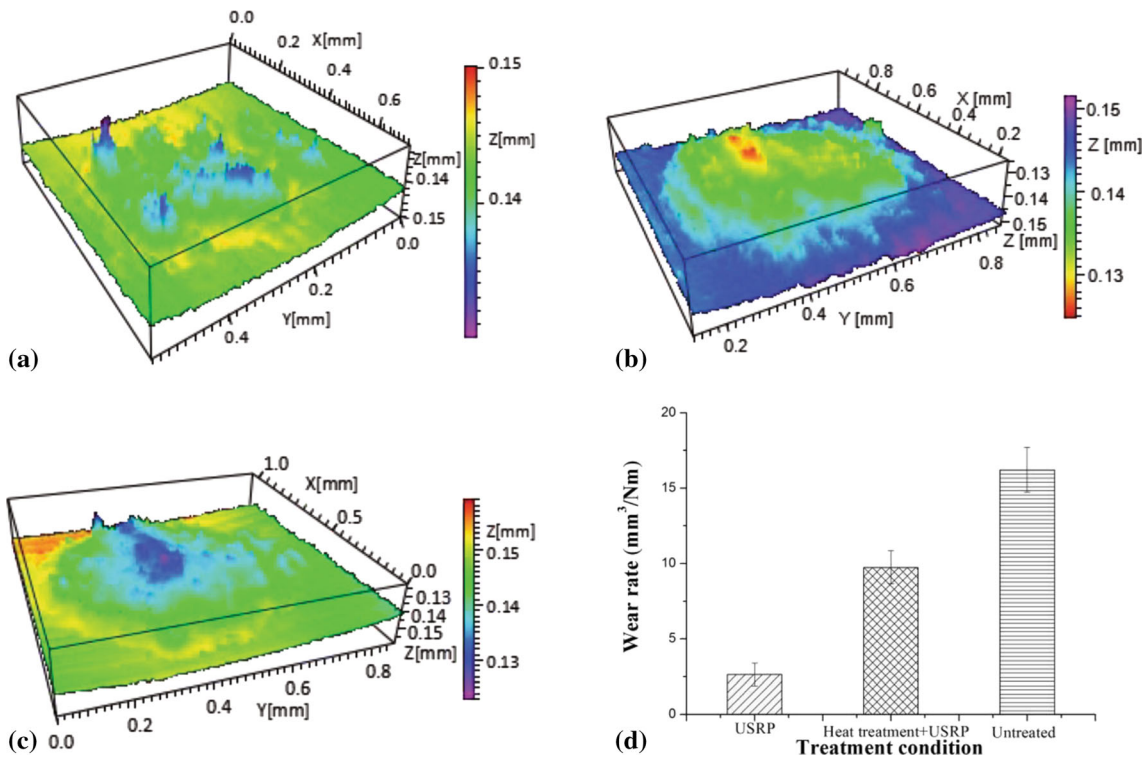


**Fig. 12** 3D wear profiles and wear rate of the samples: (a) the unheat-treated sample treated by USRP; (b) the heat-treated sample treated by USRP; (c) the untreated sample; (d) wear rate of the samples

### 3.5 Wear Rate

The 3D scanning profiles of wear scars for the samples are shown in Fig. 12. It can be found that the volume loss of USRP-treated sample is obviously smaller than that of the untreated sample. This should be attributed to surface strengthening layer produced by USRP treatment. It can significantly increase the wear resistance of the sample during fretting friction and wear test. But one obviously notable difference is that the unheat-treated sample shows the less material volume loss than the heat-treated sample under the same USRP treatment conditions. This is consistent with the actual observed wear scar surface in Fig. 8. On the one hand, the good plasticity and high compressive residual stress of unheat-treated material after USRP treatment can increase material deformation resistance and reduce crack propagation and spalling during fretting friction and wear test. On the other hand, the decrease plasticity and compressive residual stress of heat-treated material after USRP treatment will increase the proportion of abrasive wear, promote the crack propagation, and produce the more delamination spalling. Moreover, the heat-treated material treated by USRP treatment exhibits the larger grains and thinner modified layer. Finally, the combined effects of these factors aggravate the fretting wear of the heat-treated sample treated by USRP treatment and increase material wear rate. But the wear rate of the heat-treated sample is almost three times that of the unheat-treated sample in the same USRP treatment conditions (Fig. 12d). This also shows that the elastoplasticity and microstructure of the material itself have an important influence on the wear resistance of the material, and the process of USRP treatment can significantly decline the wear rate of the sample. In addition, the friction and wear properties of counter grinding sample also indirectly determine the wear rate of the target sample.

## 4. Conclusions

- (1) The sample only treated by USRP treatment shows the finer grains, the denser dislocations, and the thicker modification layer than the heat-treated sample treated by USRP treatment. The main reason is the change of microstructure caused by heat treatment and the increase of the area ratio of  $\alpha$  phase.
- (2) The heat-treated sample treated by USRP treatment has the higher surface roughness and microhardness and the lower compressive residual stress than the unheat-treated sample treated by USRP treatment. The results of fretting friction and wear test indicate that the unheat-treated sample has the lower CoF and the better wear resistance than the unheat-treated sample in the same USRP treatment conditions. The heat-treated sample processed by USRP treatment shows the serious abrasive wear and material bonding behavior.
- (3) The sliding regimes are analyzed by the changes in CoFs and fretting wear scars. Moreover, the effect of friction temperature, third body effect, and viscoplasticity on the fretting friction and wear performance are discussed under the same slip conditions. Finally, the heat-treated sample shows the larger wear rate than the unheat-treated sample under the same USRP treatment because of the change of microstructure and mechanical properties. They will intensify the friction and wear behavior between the counter grinding sample and target sample. But the wear rate of the heat-treated sample treated by USRP is still significantly less than that of the untreated sample.

## Acknowledgments

This study was funded by Doctoral Research Fund of Northeast Electric Power University (BSJXM-2019217) and Science and Technology Research Project of Jilin Provincial Department of Education (JJKH20210086KJ).

## Reference

1. K. Ren, W. Yue and H.Y. Zhang, Surface Modification of Ti6Al4V Based on Ultrasonic Surface Rolling Processing and Plasma Nitriding for Enhanced Bone Regeneration, *Surf. Coat. Technol.*, 2018, **349**, p 602–610. <https://doi.org/10.1016/j.surfcoat.2018.06.039>
2. M. Zhang, J. Deng, Z.H. Liu et al., Investigation into Contributions of Static and Dynamic Loads to Compressive Residual Stress Fields Caused by Ultrasonic Surface Rolling, *Int. J. Mech. Sci.*, 2019, **163**, 105144. <https://doi.org/10.1016/j.ijmecsci.2019.105144>
3. Y. Lu, M. Aristizabal, X. Wang et al., The Influence of Heat Treatment on the Microstructure and Properties of HIPed Ti-6Al-4V, *Acta Mater.*, 2019, **165**, p 520–527. <https://doi.org/10.1016/j.actamat.2018.12.025>
4. M. Muztahid, W.P. Jonathan, S. Nima et al., Effect of Heat Treatments on Microstructure/Small-Scale Properties of Additive Manufactured Ti-6Al-4V, *Int. J. Adv. Manuf. Tech.*, 2019, **103**(9–12), p 4161–4172. <https://doi.org/10.1007/s00170-019-03789-w>
5. G. Li, S.G. Qu, M.X. Xie et al., Effect of Multi-pass Ultrasonic Surface Rolling on the Mechanical and Fatigue Properties of HIP Ti-6Al-4V Alloy, *Materials*, 2017, **10**(2), p 133. <https://doi.org/10.3390/ma10020133>
6. X.C. Yan, S. Yin, C.Y. Chen et al., Effect of Heat Treatment on the Phase Transformation and Mechanical Properties of Ti6Al4V Fabricated by Selective Laser Melting, *J. Alloys Compd.*, 2018, **764**, p 1056–1071. <https://doi.org/10.1016/j.jallcom.2018.06.076>
7. M.K. Zhang, Y.Q. Yang, D. Wang et al., Effect of Heat Treatment on the Microstructure and Mechanical Properties of Ti6Al4V Gradient Structures Manufactured by Selective Laser Melting, *Mater. Sci. Eng. A*, 2018, **736**, p 288–297. <https://doi.org/10.1016/j.msea.2018.08.084>
8. C.S. Liu, D.X. Liu, X.H. Zhang et al., On the Influence of Ultrasonic Surface Rolling Process on Surface Integrity and Fatigue Performance of Ti-6Al-4V Alloy, *Surf. Coat. Technol.*, 2019, **370**, p 24–34. <https://doi.org/10.1016/j.surfcoat.2019.04.080>
9. A.T. Bozdana and N.N.Z. Gindy, Comparative Experimental Study on Effects of Conventional and Ultrasonic Deep Cold Rolling Processes on Ti-6Al-4V, *Mater. Sci. Technol.*, 2008, **24**(11), p 1378–1384. <https://doi.org/10.1179/174328408X302431>
10. C. Liu, D. Liu, X. Zhang et al., Improving Fatigue Performance of Ti-6Al-4V Alloy Via Ultrasonic Surface Rolling Process, *J. Mater. Sci. Technol.*, 2019, **36**(8), p 1555–1562. <https://doi.org/10.1016/j.jmst.2019.03.036>
11. D.S. She, S.H. Liu, J.J. Kang et al., Abrasive Wear Resistance of Plasma-Nitrided Ti Enhanced by Ultrasonic Surface Rolling Processing Pre-Treatment, *Materials*, 2019, **12**(19), p 3260. <https://doi.org/10.3390/ma12193260>
12. M.G. Yin, Z.B. Cai, Z.X. Zhang et al., Effect of Ultrasonic Surface Rolling Process on Impact-Sliding Wear Behavior of the 690 Alloy, *Tribol. Int.*, 2020, **147**, p 105600. <https://doi.org/10.1016/j.triboint.2019.02.008>
13. Z.J. Ren, F.Q. Lai, S.G. Qu et al., Effect of Ultrasonic Surface Rolling on Surface Layer Properties and Fretting Wear Properties of Titanium Alloy Ti5Al4Mo6V2Nb1Fe, *Surf. Coat. Technol.*, 2020, **389**, 125612. <https://doi.org/10.1016/j.surfcoat.2020.125612>
14. Y. Meng, J.X. Deng, Y. Zhang et al., Tribological Properties of Textured Surfaces Fabricated on AISI 1045 Steels by Ultrasonic Surface Rolling Under dry Reciprocating Sliding, *Wear*, 2020, **460**, 203488. <https://doi.org/10.1016/j.wear.2020.203488>
15. A. Amanov and S. Sasaki, A Study on the Tribological Characteristics of Duplex-Treated Ti-6Al-4V Alloy Under Oil-Lubricated Sliding Conditions, *Tribol. Int.*, 2013, **64**, p 155–163. <https://doi.org/10.1016/j.triboint.2013.03.015>
16. G. Li, S.G. Qu, Y.X. Pan et al., Effects of the Different Frequencies and Loads of Ultrasonic Surface Rolling on Surface Mechanical Properties and Fretting Wear Resistance of HIP Ti-6Al-4V Alloy, *Appl. Surf. Sci.*, 2016, **389**, p 324–334. <https://doi.org/10.1016/j.apsusc.2016.07.120>
17. R.K. Gupta, K.V. Anil, M.G. Christy et al., Strain Hardening of Ti-6Al-4V Sheets with Prior Heat Treatment and Cold Working, *Mater. Sci. Eng. A*, 2016, **662**, p 537–550. <https://doi.org/10.1016/j.msea.2016.03.094>
18. N. Ao, D. Liu, X. Zhang et al., Surface Nanocrystallization of Body-Centered Cubic Beta Phase in Ti-6Al-4V Alloy Subjected to Ultrasonic Surface Rolling Process, *Surf. Coat. Technol.*, 2019, **361**, p 35–41. <https://doi.org/10.1016/j.surfcoat.2019.01.045>
19. S. Jelliti, C. Richard, D. Reirant et al., Effect of Surface Nanocrystallization on the Corrosion Behavior of Ti-6Al-4V Titanium Alloy, *Surf. Coat. Technol.*, 2013, **224**, p 82–87. <https://doi.org/10.1016/j.surfcoat.2013.02.052>
20. N.R. Tao, Z.B. Wang, W.P. Tong et al., An Investigation of Surface Nanocrystallization Mechanism in Fe Induced by Surface Mechanical Attrition Treatment, *Acta Mater.*, 2002, **50**(18), p 4603–4616. [https://doi.org/10.1016/S1359-6454\(02\)00310-5](https://doi.org/10.1016/S1359-6454(02)00310-5)
21. K. Kubiak, S. Fouvry, A.M. Marechal et al., Behaviour of Shot Peening Combined with WC-Co HVOF Coating Under Complex Fretting Wear and Fretting Fatigue Loading Conditions, *Surf. Coat. Technol.*, 2006, **201**, p 4323–4328. <https://doi.org/10.1016/j.surfcoat.2006.08.094>
22. A. Amanov, I. Cho, D. Kim and Y. Pyun, Fretting Wear and Friction Reduction of CP Titanium and Ti-6Al-4V Alloy by Ultrasonic Nanocrystalline Surface Modification, *Surf. Coat. Technol.*, 2012, **207**, p 135–142. <https://doi.org/10.1016/j.surfcoat.2012.06.046>
23. Q.L. Zhang, Z.Q. Hu, W.W. Su et al., Microstructure and Surface Properties of 17-4PH Stainless Steel by Ultrasonic Surface Rolling Technology, *Surf. Coat. Technol.*, 2017, **321**, p 64–73. <https://doi.org/10.1016/j.surfcoat.2017.04.052>
24. S. Heredia and S. Fouvry, Introduction of a New Sliding Regime Criterion to Quantify Partial, Mixed and Gross Slip Fretting Regimes: Correlation with Wear and Cracking Processes, *Wear*, 2010, **269**(7–8), p 515–524. <https://doi.org/10.1016/j.wear.2010.05.002>
25. B. Wu, J.X. Zhang, L.J. Zhang et al., Effect of Ultrasonic Nanocrystal Surface Modification on Surface and Fatigue Properties of Quenching and Tempering S45C Steel, *Appl. Surf. Sci.*, 2014, **321**, p 318–330. <https://doi.org/10.1016/j.apsusc.2014.09.068>

**Publisher's Note** Springer Nature remains neutral with regard to jurisdictional claims in published maps and institutional affiliations.